

The effect of ionizing background fluctuations on the spatial correlations of high redshift Ly α -emitting galaxies

Avery Meiksin¹ * & Teresita Suarez¹

¹*SUPA†, The Royal Observatory, Edinburgh, Blackford Hill, Edinburgh EH9 3HJ, UK*

Accepted 8 August 2022. Received 5 August 2022; in original form 30 May 2022.

ABSTRACT

We investigate the possible influence of fluctuations in the metagalactic photoionizing ultra-violet background (UVBG) on the clustering of Ly α -emitting galaxies through the modulation of the ionization level of the gas surrounding the systems. At redshifts $z > 5$, even when assuming the reionization of the intergalactic medium has completed, the fluctuations are sufficiently large that they may non-negligibly enhance, and possibly even dominate, the angular correlation function on scales up to a few hundred arcsecs. Whilst a comparison with observations at $z \simeq 5.7$ is statistically consistent with no influence of UVBG fluctuations, allowing for the fluctuations opens up the range of acceptable models to include those with relatively low bias factors for the Ly α -emitting galaxies. In this case, the evolution in the bias factor of Ly α -emitters over the approximate redshift range $3 < z < 7$ corresponds to a nearly constant halo mass for Ly α -emitting galaxies of $\sim 10^{10.5} M_{\odot}$.

1 INTRODUCTION

The discovery of high redshift Ly α -emitting galaxies (Hu & McMahon 1996; Pascarelle et al. 1996) has led to a series of Ly α emitter (LAE) surveys of increasing depth (Ouchi et al. 2020). Surveys at $z > 7$ likely probe the Epoch of Reionization (EoR), when the Universe was transformed from neutral to ionized by the first galaxies and Quasi-Stellar Objects (QSOs), over a characteristic redshift range $6 \lesssim z \lesssim 10$ (Planck Collaboration 2020). LAE surveys therefore provide not only information about some of the properties of the earliest galaxies in the Universe, but also about the evolving nature of the Intergalactic Medium (IGM).

The evolution in the luminosity distribution of LAEs has been used to constrain the ionization state of the IGM during the EoR. The decrease in the LAE Ly α luminosity function compared with the ultra-violet (UV) continuum luminosity function of Lyman-break galaxies (LBGs) agrees with an increasing neutral hydrogen fraction of the IGM with redshift. The mean neutral hydrogen fraction is estimated to be $\bar{x}_{\text{HI}} > 0.1$ at $z > 6.6$ (Konno et al. 2018), and it possibly exceeds $\bar{x}_{\text{HI}} > 0.2$ at $z > 7$ (eg Itoh et al. 2018; Goto et al. 2021). The evolving rate of detection of Ly α emission in LBGs was used by Mason et al. (2018) to suggest $\bar{x}_{\text{HI}} = 0.59_{-0.15}^{+0.11}$ at $z \sim 7$.

The effects of incomplete reionization on the properties of LAEs are less able to constrain the ionization state of the IGM at $z < 6$. The strongest constraints come from the Ly α forest measured in bright, background QSOs. The distributions of the measured Ly α effective optical depths τ_{α} at $z > 5$ are unexpectedly broad compared with the predictions of numerical simulations of the IGM. The breadths of the distributions increase with redshift, with patches of high attenuation extending over $100 h^{-1}$ comoving Mpc appearing along some lines of sight at $z > 6$ (Becker et al. 2015, 2018; Bosman et al. 2018; Yang et al. 2020; Bosman et al. 2022). It has been suggested that late reionization may account for the breadths of

the Ly α effective optical depth distributions, with the EoR ending as late as $z \simeq 5.2 - 5.5$ (Kulkarni et al. 2019a; Keating et al. 2020; Nasir & D’Aloisio 2020). In this scenario, extended regions of high optical depth originate in residual patches of neutral hydrogen.

An alternative explanation suggested for the breadths of the distributions is the “dappling” of the IGM by a fluctuating metagalactic UVBG (Meiksin 2020). Fluctuations in the UVBG arise from both spatial correlations between the sources and from the shot noise due to their discreteness (Gontcho A Gontcho et al. 2014; Pontzen 2014; Suarez & Pontzen 2017; Meiksin & McQuinn 2019). Whilst the fractional contribution of QSO sources to the UV background is below half at $z > 3$ and diminishes with increasing redshift, the QSOs continue to dominate the shot noise contribution to the background. The large scale UVBG fluctuations resulting from the source shot noise reproduce the measured breadths in the distributions of the Ly α effective opacity at $3 < z < 6$.

LAEs have been measured to cluster spatially. The strength of the clustering has been used to infer the nature of LAEs from the estimated bias factors. Comparison with the expected clustering of dark matter shows an increase in the LAE bias from $b_L \sim 1.5$ at $z < 4$ to as high as $b_L \sim 6$ at $z > 5$, with inferred dark matter halo masses of $10^{10.3} - 10^{11.3} M_{\odot}$ and a duty cycle, representing the fraction of haloes in a LAE phase, of less than 1% (Ouchi et al. 2018). From the evolution of the bias factor, Ouchi et al. (2018) infer LAEs at $z > 2$ may be the progenitors of massive elliptical galaxies today. The estimates of the LAE bias factors, however, show considerable scatter at the higher redshifts, with estimates for b_L at $z = 5.7$ ranging between 4.1 ± 0.2 and 6.1 ± 0.7 , and at $z = 6.6$ between $b_L = 3.6 \pm 0.7$ and 4.5 ± 0.6 , depending on the field(s) analysed (Ouchi et al. 2010, 2018). The origin of the discrepant values, especially at $z = 5.7$, is unclear. It has been suggested that results for some of the smaller fields may be affected by cosmic variance (Kusakabe et al. 2018),

with the clustering in one field at $z = 5.7$ dominated by a protocluster (Ouchi et al. 2010). Firmly establishing the evolution of the LAE bias factors will help elucidate the nature of the host systems at high redshifts and of their counterparts today.

The interpretation of the clustering signal is also complicated by the possible effects of Ly α photon scattering by the intervening IGM. The clustering of LAEs at $z > 5$ may depend on the physical character of the EoR through the ionization structure of the IGM. The patchwork of ionized and still-neutral regions during the EoR will be imprinted on the spatial correlations of LAEs because of the relative difference in attenuation of the Ly α emission line of the galaxies in different patches (Furlanetto et al. 2006; McQuinn et al. 2007). Comparison with observations suggests a mean IGM neutral hydrogen fraction below 30% at $z = 6.6$ (Ouchi et al. 2018).

The clustering of LAEs may also depend on radiative transfer effects on the sample selection, since the Ly α emission line may be modulated by scattering through the intervening IGM, which traces the same dark matter density field as do the galaxies (Wyithe & Dijkstra 2011; Zheng et al. 2011; Gurung-López et al. 2020). Local non-linear redshift space distortions may further confound interpretation of the clustering strength (Byrohl et al. 2019).

In this paper, we suggest that another factor governing the clustering of LAE systems are fluctuations in the UVBG after the end of cosmic reionization. The gas surrounding a LAE may give rise to a non-negligible Ly α optical depth redward of the Ly α emission line (eg Verhamme et al. 2006; Laursen et al. 2011). UVBG fluctuations will then modify the detectability of the systems and imprint their spatial correlations on the spatial correlation function of the LAEs. We assess the possible contribution of UVBG fluctuations to the spatial correlations of LAEs, and constrain the attenuating properties of the gas surrounding the LAEs. We shall show that allowing for UVBG fluctuations increases the uncertainty in the LAE bias factors inferred from the angular correlation function.

Modelling the effect of the UVBG on the spatial correlations of LAEs, however, is hampered by two difficulties: (1) the rarity of the QSOs at high redshift requires either very large simulation volumes, on the order of $800h^{-1}$ Mpc (comoving) or very many statistical realisations in smaller volumes, to capture the shot-noise contribution (Meiksin 2020), and (2) the origin and subsequent radiative transfer of the Ly α emission line from LAEs is unknown. We overcome the first difficulty by using a perturbative approach to model the UVBG fluctuations (Meiksin & McQuinn 2019), as the underlying density fluctuations are small over the physical scales for which we estimate the LAE spatial correlations. The latter difficulty includes uncertainties in the amount of obscuration of the escaping Ly α photons from the unknown clumpiness and flow pattern of the surrounding circumgalactic and intergalactic media. We adopt a simple statistical model described below to assess the amount of obscuration of the Ly α emission line by the gas surrounding LAEs. The combined model is designed to capture the range of possible impact the UVBG fluctuations may have on the LAE spatial correlations.

The paper is organised as follows. In the next section, we describe our model for assessing the possible effect of UVBG fluctuations on the measured angular correlation function of LAEs. In Sec. 3, comparisons between the model predictions and measurements are presented. We discuss these in Sec. 4,

and provide a summary of our conclusions in the last section. A flat cosmology is assumed with $\Omega_m = 0.31$, $\sigma_8 = 0.81$ and $n = 0.97$ (Planck Collaboration 2020).

2 THE MODEL

2.1 UV background model

The mean photoionizing UVBG is modelled following Meiksin & McQuinn (2019) and Meiksin (2020), with some recent updates. In brief, both galactic and QSO sources are included in the mean metagalactic emissivity. The evolving Schechter luminosity function fit from Bouwens et al. (2015) is adopted for the galactic contribution. We use Model 3 of Kulkarni et al. (2019b) for the QSO luminosity function, confined to sources with absolute AB magnitudes at 1450 Å of $-30 < M_{1450} < -21$. The mean free path of ionizing photons at the Lyman photoelectric edge is taken from Worseck et al. (2014) for $z < 5$ and Becker et al. (2021) for $z \geq 5$. The mean metagalactic emissivity at the Lyman edge is adjusted to reproduce the median effective IGM Ly α optical depth measurements listed in Meiksin (2009) for $z < 5$, and from Bosman et al. (2018) for $5 \leq z < 5.4$ and Yang et al. (2020) for $z \geq 5.4$.

The fluctuations in the UVBG arise from fluctuations in the Lyman continuum opacity of the IGM, and from the spatial clustering of the sources and the source shot noise. We assume a galaxy bias factor $b_G = 3$ (e.g. Bielby et al. 2013), noting it may be higher at $z > 5$. An evolving bias factor is adopted for the QSOs of $b_Q = 0.278(1+z)^2 + 0.57$ (Laurent et al. 2017). At $z > 5$, the fluctuations are dominated by the shot noise in the QSO counts over the scales of interest. For a short source lifetime compared with the age of the Universe, the shot noise contribution is proportional to the source lifetime. For a long lifetime, the shot noise is given by the steady-state limit.

Following Meiksin & McQuinn (2019), we define the following quantities: for an UVBG intensity I_ν , emissivity j_ν and photoelectric cross section σ_ν , $f = \int d\nu (I_\nu/h_P\nu)\sigma_\nu$, $j = \int d\nu (j_\nu/h_P\nu)\sigma_\nu$ and $\zeta = \langle I_L \rangle \sigma_L / h_P \langle f \rangle$, where h_P is Planck's constant and I_L and σ_L are the values of the intensity and cross section at the Lyman edge, respectively. Here, $\langle \dots \rangle$ denotes a spatial average. A dimensionless opacity $\chi = (c/H) \langle \alpha_{\text{eff}} \rangle$ is also defined, where α_{eff} is the frequency-averaged opacity weighted by $I_\nu \sigma_\nu / h_P \nu$, and H is the Hubble parameter. The dimensionless ratio $\phi = c \langle j \rangle / [H(\chi + \zeta) \langle f \rangle]$ describes the evolution of the radiation field. For a non-evolving radiation field, $\phi = 1$. The mean metagalactic photoionization rate is related to f by $\Gamma = 4\pi \langle f \rangle$. The Fourier component for comoving wavenumber k of the perturbation to the photoionization rate is given in the steady-state limit by

$$\tilde{\delta}_{\Gamma, \text{SS}}(\kappa) = \frac{\phi(\chi + \zeta)\tilde{\delta}_j(\kappa) - b_{\chi, \delta}\chi\tilde{\delta}(\kappa)}{\frac{\kappa}{a} \left[\text{atan}\left(\frac{\kappa}{a\phi(\chi + \zeta)}\right) \right]^{-1} + b_{\chi, \Gamma}\chi}, \quad (1)$$

where $\tilde{\delta}_j$ and $\tilde{\delta}$ are the perturbations in the source density and gas density respectively, $\kappa = (c/H)k$ is a dimensionless comoving wavenumber, and $a = 1/(1+z)$. Here, $\tilde{\delta} \log \chi = b_{\chi, \delta}\tilde{\delta} + b_{\chi, \Gamma}\tilde{\delta}_\Gamma$. Eq. (1) is similar to the findings of Gontcho A Gontcho et al. (2014) and Pontzen (2014), who both additionally assume $\phi = 1$. The power spectrum of the light fluctuations in a comoving volume V_u is $P_\Gamma^{\text{SS}}(k) = V_u \langle \tilde{\delta}_\Gamma^\dagger(k) \tilde{\delta}_\Gamma(k) \rangle^{\text{SS}}$.

In addition to a component proportional to the dark matter power spectrum and dependent on the bias factors of the sources, a source shot noise term also contributes additively to the full power spectrum. The shot noise contribution is given by

$$V_u \langle \tilde{\delta}_\Gamma^*(k) \tilde{\delta}_\Gamma(k) \rangle_{\text{shot}}^{\text{SS}} \sim \left[\frac{\pi}{2} \phi(\chi + \zeta) \frac{a}{\kappa} \right]^2 \frac{1}{n_{\text{eff}}}, \quad (2)$$

in the limit $\kappa \gg 1$, corresponding to modes with wavelengths short compared with the cosmological horizon. The effective number density of the sources is given by $n_{\text{eff}} = \langle L \rangle_\Phi^2 / \langle L^2 \rangle_\Phi$, where the averages $\langle \dots \rangle_\Phi$ are carried out over the luminosity density $\Phi(L)$ of the sources.

For sources with finite lifetimes τ_S , the shot noise contribution may be substantially reduced. We adopt an approximate form which accurately interpolates between the $\kappa \ll 1$ and $\kappa \gg 1$ limits,

$$V_u \langle \tilde{\delta}_\Gamma^*(k) \tilde{\delta}_\Gamma(k) \rangle_{\text{shot}} \simeq \frac{1}{A} \frac{[\phi(\chi + \zeta)]^2}{1 + [\kappa/\kappa_*^{\text{SN}}(\kappa)]^2} \frac{1}{n_{\text{eff}}}, \quad (3)$$

where

$$A = \frac{2}{H\tau_S} \left[(\phi + b_{\chi,\Gamma})\chi + \phi\zeta + \frac{3}{4} - \frac{1}{2}\alpha_n \right] - \left[\frac{4}{\pi^2} (\phi(\chi + \zeta) - 1/2) + b_{\chi,\Gamma}\chi \right]^2, \quad (4)$$

for the approximation $n_{\text{eff}} \sim (1+z)^{-\alpha_n}$, and $\kappa_*^{\text{SN}}(\kappa) = 2\pi[c/H(z)]/[(1+z)\lambda_*^{\text{SN}}(\kappa)]$ with

$$\lambda_*^{\text{SN}} = \frac{4}{H} A^{-1/2} \times \left\{ 1 + \frac{\pi}{2} \left[\frac{4}{\pi^2} (\phi(\chi + \zeta) - 1/2) + b_{\chi,\Gamma}\chi \right] \frac{a}{\kappa(a)} \right\}, \quad (5)$$

for $H\tau_S \ll 1$ (Meiksin & McQuinn 2019). When the distance light travels during the source lifetime exceeds the mean free path of the ionizing radiation, the steady-state value is a good approximation. On scales small compared with the light travel distance over the source lifetime, $k \gg 1/(c\tau_S)$, Eq. (3) goes over to Eq. (2). Additional suppression of the power spectrum of UVBG fluctuations may arise if QSOs emit in tight beams (Suarez & Pontzen 2017); this effect is not included here.

When including the UVBG fluctuations, we adjust the escape fraction of ionizing photons from galaxies to match the median optical depth measurements. In practice this has only a small effect on the shot noise contribution because it is dominated by the QSOs.

2.2 Observed Ly α emission line

Modelling the Ly α emission line is more problematic. The observed line depends on the emission line mechanism and the subsequent Ly α radiative transfer both within and near the Ly α -emitting galaxy and through the IGM. The emission line may originate in a compact region or from several regions extending across the galaxy, which will affect the line profile generated. This will also affect the Ly α radiative transfer through the interstellar medium of the galaxy, which may be static or moving, possibly in a wind. The profile will be further modified by the gas in the circumgalactic medium (CGM) of the galaxy, and whether the gas is expanding in

a wind or infalling, and possibly part of an H II region produced by the LAE. The possible presence of dust absorption is still another complicating factor. All of these factors may vary with time over the lifetime of an individual LAE, and between different LAEs, possibly dependent on properties of the host galaxy such as its mass.

The astrophysical effects are clearly well beyond definitive detailed modelling given the current understanding of the physical properties of LAEs and their immediate environments. Several detailed Ly α radiative transfer computations have been performed of the emission line leaving the galaxy and its CGM under varying assumptions. Whilst the radiative transfer through an optically thick slab results in a double-horned emission line profile (Harrington 1973), radiative transfer through a wind or accretion flow generally suppresses either the blue side in a wind (Verhamme et al. 2006), or the red side in an accretion flow (Dijkstra et al. 2006; Verhamme et al. 2006), producing emission that is redward dominated in the case of outflow or blueward dominated in the case of infall. Backscattering off the far-side of the gas relative to the observer results in peaks displaced by as much as twice the outflow or infall velocities, possibly achieving offsets as great as $\pm 400 \text{ km s}^{-1}$ (Verhamme et al. 2006).

The details of the emission line profile are sensitive to the origin of the emission (central point source or extended emitting region), the total H I column density, the gas temperature and the expansion or infall velocity, as well as broadening by any turbulence that may be present. For emission through an expanding shell, and depending on the H I column density, for a sufficiently large expansion velocity the redward lobe splits into two, one peaking at about twice the wind velocity redward of line centre and the other just shortward of line centre (Verhamme et al. 2006). The profile also may depend on the orientation of the LAE. For photons generated within a gaseous disk, when viewed face-on the profile may be dominated by a single lobe, either blueward of line centre if the source is at the centre of an accretion flow, or redward if at the centre of a wind. When viewed edge-on, however, the profile may split into two lobes around line centre for a sufficiently high internal H I column density (eg Verhamme et al. 2012).

In reionization simulations, various approaches have been taken to model the Ly α profiles including the effect of IGM attenuation. These typically assume complete suppression of any feature blueward of the systemic Ly α wavelength of a LAE, and partial attenuation of the redward feature by the damping wing from neutral patches in the IGM (Furlanetto et al. 2006; McQuinn et al. 2007; Iliiev et al. 2008; Dijkstra et al. 2011). As we are considering the effects of IGM attenuation after reionization has completed, such a simplified treatment is inappropriate. Instead the emission line is attenuated using the mean IGM transmission $e^{-\tau_\alpha}$ at the cosmological redshift of the LAE. How much of the profile is attenuated, however, depends on several factors: the centroid of the emission line compared with the systemic velocity of the LAE, the peculiar velocity of the LAE, the size of a possible H II region produced by the LAE, gaseous outflow produced by winds from the hosting galaxy, and cosmological infall around the LAE. The latter, in particular, can result in attenuation even when the emission line is redward of the systemic velocity of a comoving LAE (Laursen et al. 2011; Weinberger et al. 2018). The detailed study of Laursen et al. (2011) shows IGM

attenuation on both the blue and red sides of the local cosmological restframe Ly α wavelength, extending redward by more than 200 km s⁻¹ at $z = 5.8$ in an early reionization scenario (with characteristic reionization redshift $z_{\text{ri}} = 10$) and to over 600 km s⁻¹ for late reionization ($z_{\text{ri}} = 6$) (their figures 3 and 4). Typically three-quarters of the Ly α radiation emergent from the galaxy is scattered out of the line of sight by the large-scale IGM for the early reionization scenario. The measured Ly α luminosity is highly sensitive to galaxy mass and the profile of the emission line emerging from the galaxy, whilst the amount further attenuated by the IGM varies widely, depending on the line of sight (their figure 8).

For simplicity we model the emission line as a single gaussian profile of width σ_l . Although the profile should split into two lobes for a LAE viewed edge-on, we treat it as unresolved, as it will make no difference to the total Ly α luminosity of a symmetric feature: the blueward half of the emission line will be suppressed by roughly the same factor. We allow the centroid to be displaced relative to the restframe Ly α attenuation edge of the IGM. In the event LAEs photoionize their surroundings, the displacement is relative to the near (lower redshift) edge of the H II bubble.

The effect of the IGM attenuation is to alter the intrinsic luminosity L of the Ly α emission line, giving the observed value

$$L_{\text{obs}} = \frac{L}{1+f} (1 + f e^{-\tau\alpha}). \quad (6)$$

For a gaussian emission line profile with velocity centroid v relative to the IGM attenuation edge and width σ_l , the factor f is given by

$$f(v) = \frac{1 - \text{erf}\left(\frac{v}{2^{1/2}\sigma_l}\right)}{1 + \text{erf}\left(\frac{v}{2^{1/2}\sigma_l}\right)}. \quad (7)$$

In the limit $v \gg \sigma_l$ (eg, wind-dominated emission), $f \rightarrow 0$ and $L_{\text{obs}} \rightarrow L$, while for $-v \gg \sigma_l$ (eg, infall-dominated emission), $f \rightarrow \infty$ and $L_{\text{obs}} \rightarrow L e^{-\tau\alpha}$. In the limit of a small velocity offset $|v| \ll \sigma_l$, $f \rightarrow 1$ (eg, as for a disk seen edge-on), and $L_{\text{obs}} \rightarrow L(1 + e^{-\tau\alpha})/2$.

We show below that only in the presence of substantial IGM attenuation will UVBG fluctuations have much of an effect on the angular correlation function of the LAEs. At moderate redshifts ($z \sim 3$), little effect is expected; but the effects may be strong at $z > 5$. In accordance with simulations of the IGM attenuation discussed above, the IGM attenuation edge may be displaced substantially redward of the cosmological restframe Ly α wavelength at these redshifts. The characteristic LAE emission line FWHM at $z = 5.7$ is 265 ± 37 km s⁻¹ (Ouchi et al. 2010), corresponding to $\sigma_l \simeq 110$ km s⁻¹. The combined displacement redward of the LAE emission line may be by as much as four times this value, allowing also for infall. Whilst there is evidence that the Ly α emission line itself is redshifted relative to the systemic velocity of the Ly α -emitting galaxy (eg McLinden et al. 2011; Verhamme et al. 2018), the observations are largely at $z \sim 3 - 4$, when winds may be driven by higher rates of star formation in more massive systems. Many of the systems also show blueward emission, although at a level consistent with outflows. It is unknown whether the Ly α emission is redshifted compared to the systemic velocity of most LAEs at $z > 5$, but even if so, it is unknown whether the gaseous surroundings at these

redshifts are outflowing, or dominated by cosmic accretion. If outflows dominate, then no strong contribution of UVBG fluctuations to the clustering of the LAEs is expected. Observations suggest the impact of intervening IGM scattering on the measured Ly α profile of LAEs increases with redshift (Hayes et al. 2021).

2.3 Spatial correlations of Ly α emitters

The effect of fluctuations in the density field and the UVBG on the number counts of LAEs may be quantified using the LAE luminosity distribution. This is well fit by a Schechter function (Ouchi et al. 2020). Since the luminosity detection threshold¹ is small compared with the exponential cut-off in the Schechter function, the total number of detected systems may be approximated as a power-law $dN/dL = n_* L^\alpha$ for LAE Ly α luminosity L . These systems will dominate the spatial correlation signal unless the high luminosity systems cluster much more strongly than the low. There is some evidence for a statistical correlation between clustering strength and LAE luminosity at $z < 5$ (Ouchi et al. 2003, 2005), but this may arise from AGN, which are not in as great abundance among LAEs at higher redshifts (Ouchi et al. 2008).

To allow for the line-of-sight variation in the amount of IGM attenuation, we model the relative offset between the LAE emission line and IGM attenuation edge as a gaussian random process with centroid velocity offset v_0 and dispersion σ_v . The observed distribution is then given by

$$\frac{dN}{dL_{\text{obs}}} = \frac{1}{(2\pi\sigma_v^2)^{1/2}} \int_{-\infty}^{\infty} dv e^{-(v-v_0)^2/2\sigma_v^2} \frac{dN}{dL} \Big|_{L(v|L_{\text{obs}})} \frac{dL}{dL_{\text{obs}}}(v), \quad (8)$$

where $L(v|L_{\text{obs}})$ is the intrinsic Ly α luminosity L required to obtain an observed luminosity L_{obs} given a velocity offset v , according to Eqs. (6) and (7). The number of systems above a particular observed value L_0 becomes (for $\alpha < -1$),

$$\mathcal{N}(L_{\text{obs}} > L_0) \simeq -\frac{\bar{n}_*}{\alpha + 1} L_0^{\alpha+1}, \quad (9)$$

where, using Eq. (8),

$$\bar{n}_* = \frac{n_*}{(2\pi\sigma_v^2)^{1/2}} \int_{-\infty}^{\infty} dv e^{-(v-v_0)^2/2\sigma_v^2} \left[\frac{1+f(v)}{1+f(v)e^{-\tau\alpha}} \right]^{\alpha+1}. \quad (10)$$

Good fits to the observed distribution of LAE luminosities are provided by $\alpha = -1.8$ for $z \leq 5.7$ and $\alpha = -2.5$ for $z \geq 5.7$ (Ouchi et al. 2020).

Assuming n_* is proportional to the local cosmological mass density, the perturbation in the number of detected LAEs, allowing for both mass density and UVBG fluctuations, is then given by

$$\frac{\delta\mathcal{N}}{\mathcal{N}}(\mathbf{k}, z) = [b_L + f(\Omega_m)\mu_k^2] \hat{\delta}(\mathbf{k}, z) + (\alpha+1)g(v, \tau_\alpha)\hat{\delta}\tau_\alpha(\mathbf{k}, z), \quad (11)$$

¹ The detection threshold is in practice based on equivalent width. We simplify the analysis by formulating the detection in terms of a luminosity threshold.

The effect of ionizing background fluctuations on the spatial correlations of high redshift Ly α -emitting galaxies

where b_L is the cosmological density bias factor for the LAEs and

$$g(v_0, \tau_\alpha) = \frac{\int_{-\infty}^{\infty} dv e^{-\frac{(v-v_0)^2}{2\sigma_v^2}} \left[\frac{1+f(v)}{1+f(v)e^{-\tau_\alpha}} \right]^{\alpha+1} \frac{f(v)e^{-\tau_\alpha}}{1+f(v)e^{-\tau_\alpha}}}{\int_{-\infty}^{\infty} dv e^{-\frac{(v-v_0)^2}{2\sigma_v^2}} \left[\frac{1+f(v)}{1+f(v)e^{-\tau_\alpha}} \right]^{\alpha+1}}. \quad (12)$$

This provides a convenient parametrisation of the influence of UVBG fluctuations on the LAE correlation function in that g is confined to the range $0 \leq g \leq 1$. For simplicity, unless stated otherwise, we take the same width for the velocity offset gaussian as for the line profile ($\sigma_v = \sigma_l$). This avoids a partial degeneracy between the offset of the centroid and the width of the distribution. Although we use the full integration in Eq. (12) for all results presented below, we note that at $z = 5.7$ and for $\alpha = -1.8$, g is well-approximated over $-4\sigma_l < v_0 < 0$ by

$$g(v_0, z = 5.7) \simeq \frac{1}{2} \left[1 - \tanh \left(\frac{3 + v_0/\sigma_l}{2^{1/2}} \right) \right]. \quad (13)$$

The additional term $f(\Omega_m)\mu_k^2$ in Eq. (11) accounts for redshift space distortions (Kaiser 1987), where $f(\Omega_m)$ is the dimensionless linear growth rate of the density fluctuation growing mode (a flat Universe is assumed) and $\mu_k = \hat{\mathbf{n}} \cdot \mathbf{k}$ for line-of-sight direction $\hat{\mathbf{n}}$.

The LAE power spectrum, allowing for both density and UVBG fluctuations and for redshift space distortions, is then

$$\begin{aligned} P_L(k, \mu_k, z) &= V_u \left\langle \frac{\delta \hat{\mathcal{N}}^*}{\mathcal{N}}(\mathbf{k}, z) \frac{\delta \hat{\mathcal{N}}}{\mathcal{N}}(\mathbf{k}, z) \right\rangle \\ &= b_{\text{eff}}^2 V_u \left\langle \hat{\delta}^*(\mathbf{k}, z) \hat{\delta}(\mathbf{k}, z) \right\rangle \left[1 + \frac{f(\Omega_m)}{b_{\text{eff}}} \mu_k^2 \right]^2 \\ &+ b_{\alpha, \Gamma} (\alpha + 1) g \tau_\alpha b_{\text{eff}} V_u \left\langle \hat{\delta}_\Gamma^*(\mathbf{k}, z) \hat{\delta}(\mathbf{k}, z) \right\rangle \\ &+ \left\langle \hat{\delta}_\Gamma(\mathbf{k}, z) \hat{\delta}^*(\mathbf{k}, z) \right\rangle \left[1 + \frac{f(\Omega_m)}{b_{\text{eff}}} \mu_k^2 \right] \\ &+ [b_{\alpha, \Gamma} (\alpha + 1) g \tau_\alpha]^2 V_u \left\langle \hat{\delta}_\Gamma^*(\mathbf{k}, z) \hat{\delta}_\Gamma(\mathbf{k}, z) \right\rangle \end{aligned} \quad (14)$$

where

$$b_{\text{eff}} = b_L + b_{\alpha, \delta} (\alpha + 1) g \tau_\alpha, \quad (15)$$

and we have introduced the bias factors $b_{\alpha, \delta} = d \log \tau_\alpha / d \log \rho_b$ and $b_{\alpha, \Gamma} = d \log \tau_\alpha / d \log \Gamma$, where ρ_b is the baryon density. The factor b_{eff} includes the radiative transfer selection effect on the LAE sample discussed by Zheng et al. (2011) and Wyithe & Dijkstra (2011), as an enhancement in the IGM density reduces the detectability of a LAE. For $\alpha < -1$, this results in a suppression of the LAE clustering signal. Because fluctuations in the UVBG will also affect τ_α , additional terms proportional to $b_{\alpha, \Gamma}$ contribute. These arise from fluctuations in the mean free path of Lyman continuum photons and from fluctuations in the spatial density of the radiation sources, here assumed to trace the underlying dark matter density field. The additional contributions are proportional to $\hat{\delta}_\Gamma^* \hat{\delta}$ (and its complex conjugate). Another contribution arises from the shot noise of the sources, which is included in the term proportional to $\hat{\delta}_\Gamma^* \hat{\delta}_\Gamma$. (See Meiksin & McQuinn 2019, for details.)

The values for $b_{\alpha, \delta}$ and $b_{\alpha, \Gamma}$ are computed for the log-normal approximation model for the Ly α forest described in Meiksin (2020), for which the baryon fluctuations are the same as the dark matter fluctuations over the length scales of interest (large compared with the Jeans length of the IGM). The redshift dependences of the coefficients are well fit over $2 < z < 6$ by

$$b_{\alpha, \delta} \simeq -0.07834(1+z) + 1.12334$$

and

$$b_{\alpha, \Gamma} \simeq 0.07645(1+z) - 0.71815.$$

The computation of the predicted angular correlation function is facilitated by decomposing the power spectrum, including redshift space distortions, into its Legendre components

$$P_l(k, z) = \frac{2l+1}{2} \int_{-1}^1 d\mu_k P_L(k, \mu_k, z) L_l(\mu_k), \quad (16)$$

(Hamilton 1998), where $L_l(\mu_k)$ is a Legendre polynomial of order l . In the linear density approximation (and assuming a flat sky) only the $l = 0, 2$ and 4 components are non-vanishing. The Legendre components of the redshift-space correlation function corresponding to the power spectrum components are given by

$$\xi_l(r, z) = \frac{i^l}{2\pi^2} \int_0^\infty dk k^2 j_l(kr) P_l(k, z). \quad (17)$$

The angular dependence may be recovered through

$$\xi(r, \mu, z) = \sum_{i=0}^2 L_{2i}(\mu) \xi_{2i}(r, z), \quad (18)$$

where $\mu = \hat{\mathbf{n}} \cdot \hat{\mathbf{r}}$ for two points separated by \mathbf{r} . The angular correlation function at redshift z for objects separated by a ray with projected separation $b_\perp \simeq D_A \theta$ (in the small angle approximation) relative to the line of sight from the observer is then

$$\omega(\theta, \mu) \simeq \sum_{i=0}^2 \xi_{2i}(D_A [1+z] \theta / [1-\mu^2]^{1/2}) L_{2i}(\mu), \quad (19)$$

where D_A is the angular-diameter distance to redshift z and μ is the cosine of the angle between the ray connecting the objects and the line of sight. The redshift factor $[1+z]$ multiplying D_A is introduced since k and r are assumed to be in comoving units in Eq. (17).

Measurements of the angular correlation function of LAEs are carried out for systems confined to redshift shells defined by the narrow-band filter used for measuring the Ly α emission line. A shell of width Δz in redshift corresponds to a comoving width $\Delta l = (c/H)\Delta z$. To compute the angular correlation function in a shell of width Δz , the spatial correlations must be averaged along the line of sight through the shell:

$$\omega(\theta) \simeq \frac{2}{\Delta l} \sum_{i=0}^2 \int_0^{\Delta l/2} dl \xi_{2i}(l/\mu) L_{2i}(\mu), \quad (20)$$

where $\mu = l / [l^2 + (D_A [1+z] \theta)^2]^{1/2}$.

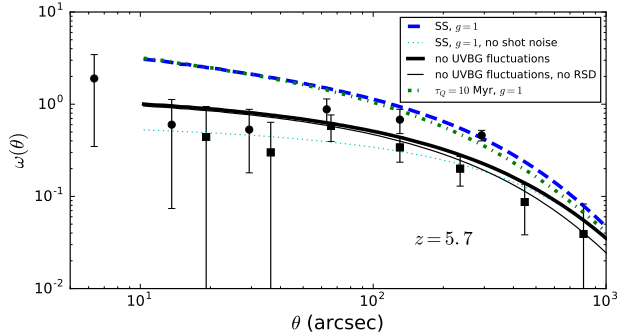


Figure 1. LAE angular correlation function at $z = 5.7$ for LAE bias factor $b_{\text{LAE}} = 4.1$ and allowing for the maximum effect of UVBG fluctuations ($g = 1$). Results are shown in the steady-state limit with the contribution from source shot noise (long-dashed blue curve) and without (dotted cyan curve), and for time varying UVBG fluctuations with a QSO lifetime $\tau_Q = 10$ Myr (dot-dashed green curve). Also shown is the result for no UVBG fluctuations, (solid black curves; the lighter curve is without redshift space distortions). The data points are taken from Ouchi et al. (2020), based on the samples analysed in Ouchi et al. (2010) (circles) and Ouchi et al. (2018) (squares). (At $z = 5.7$, 100 arcsecs corresponds to a comoving separation of $2.7h^{-1}$ Mpc.)

3 RESULTS

We first consider the limiting case $g = 1$ for the expected angular correlation function of LAEs, corresponding to $-v_0 \gg \sigma_l$ and $f \rightarrow \infty$, so that the entire emission line is attenuated, giving the maximal signature of UVBG fluctuations on the spatial correlations of the LAEs. For $z < 5$, we find the contribution from UVBG fluctuations is negligible (less than 2%), but the contribution grows rapidly with redshift as a result of the rapidly rising intergalactic effective Ly α optical depth.

In Fig. 1, we show the effect of UVBG fluctuations with $g = 1$ on the angular correlation function at $z \simeq 5.7$, matching a redshift value for LAEs measured in the SILVERRUSH Subaru survey (Ouchi et al. 2018). We average the spatial correlations over a redshift shell $\Delta z \simeq 0.092$ wide, corresponding to the width of the narrow-band filter used in the survey. Two models for the UVBG fluctuations are illustrated, one for the steady-state limit and a second time-dependent model with a QSO source lifetime of $\tau_Q = 10$ Myr. (The lifetime of the galaxies is taken to be 100 Myr, but the finite value has a negligible effect on the UVBG fluctuations because of the high abundance of the galaxies.) Also shown (black solid curves) is a model with no UVBG fluctuations using the best estimate LAE bias factor from Ouchi et al. (2018) of $b_L = 4.1$. The light curve does not include redshift space distortions, which enhance the angular correlations on large angular scales.²

The UVBG fluctuations greatly boost the correlations on

² This unintuitive result perhaps deserves some explanation. For small angular separations, the displacement between most pairs lies nearly along the line of sight, so that $\mu \approx 1$ and $\xi(r, \mu, z) \rightarrow \xi(r, 1, z) = \xi_0(r, z) + \xi_2(r, z) + \xi_4(r, z)$. For large angular separations, the displacements between pairs are mainly orthogonal to the line of sight, so that $\mu \approx 0$ and $\xi(r, \mu, z) \rightarrow \xi(r, 0, z) = \xi_0(r, z) - \xi_2(r, z)/2 + 3\xi_4(r, z)/8$. Without redshift space distortions $\xi_2 = \xi_4 = 0$, and $\xi = \xi_0$. Whilst allowing for redshift space

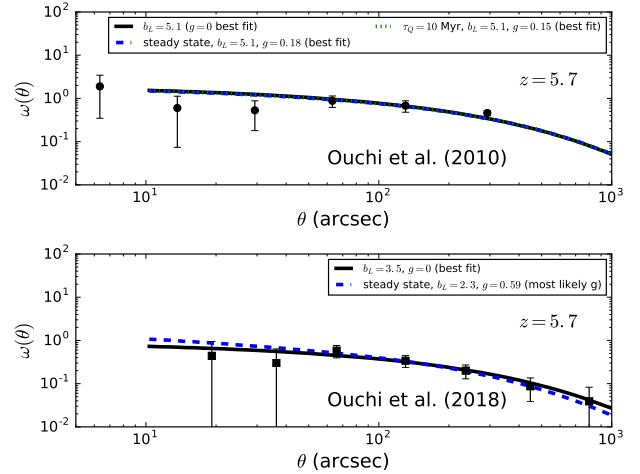


Figure 2. Best fit models to the measured LAE angular correlation functions at $z = 5.7$. Upper panel: Comparison with the data from Ouchi et al. (2010). Models are shown without UVBG fluctuations ($g = 0$; solid black curve), the steady-state model (dashed blue curve), and allowing for UVBG fluctuations for a QSO lifetime $\tau_Q = 10$ Myr (dotted green curve). Lower panel: Comparison with the data from Ouchi et al. (2018). Models are shown without UVBG fluctuations ($g = 0$; solid black curve) and the best-fitting steady-state model for the most likely value of g , marginalised over b_L , corresponding to $b_L = 0.23$ and $g = 0.59$ (dashed blue curve).

angular scales $\theta < 1000$ arcsec. The enhancement arises primarily from the source shot noise contribution to the UVBG fluctuations. For a QSO lifetime of $\tau_Q = 10$ Myr, the resulting angular correlation function is slightly smaller than for the steady-state limit. Decreasing the QSO lifetime further reduces the strength of the correlations on large angular scales, with the angle beyond which the correlations are weakened decreasing with decreasing source lifetime (not shown). Reducing the LAE bias factor b_L diminishes the strength of the correlations on large angular scales, with little change at small angles, where the UVBG fluctuation contribution dominates. It is noteworthy that the UVBG fluctuations excluding the source shot noise contribution results in a reduction in the strength of the correlations on scales smaller than a few hundred arcsecs compared to the case with no UVBG fluctuations (dotted cyan curve). This is because the effective bias factor b_{eff} in Eq. (15) is reduced below b_L by the UVBG fluctuations for $\alpha < -1$: overdense regions give rise to an excess in IGM attenuation that suppresses the detection of LAEs.

The models are fit to the data by minimising $\chi^2(b_L, g) = \sum_i [\omega_m(\theta_i) - \omega_d(\theta_i)]^2 / \sigma_{d,i}^2$, where ω_m is the model prediction for the angular correlation function and ω_d and σ_d are the measured value and its error (Ouchi et al. 2018, 2020). Marginalised probability distributions for b_L or g are computed by integrating the extraneous variable over the likelihood $\mathcal{L} = \exp[-\chi^2(b_L, g)/2]$.

Best fits to the measured correlations at $z = 5.7$ (including the integral correction for the finite survey areas), are shown in Fig. 2, using the measured values from Ouchi et al. (2010) (O10) and Ouchi et al. (2018) (O18). The point from

distortions boosts ξ_0 , the boost is largely cancelled by $\xi_2(< 0)$ in $\xi(r, 1, z)$ on the scales of interest. By contrast, ξ_2 boosts $\xi(r, 0, z)$.

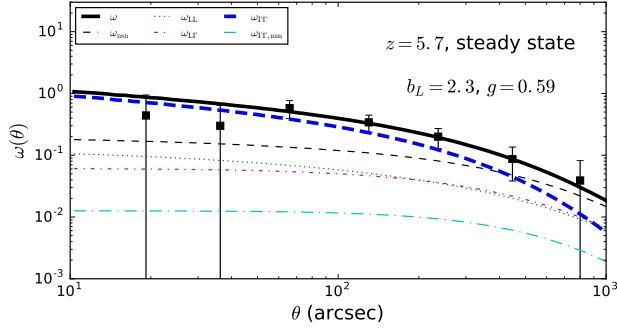


Figure 3. The break down into component contributions to $\omega(\theta)$ for the steady-state model with $b_L = 2.3$ and $g = 0.59$. Shown are the total ω (solid black curve), the total ω_{nsn} excluding the source shot noise contribution to the UVBG fluctuations (short-dashed black curve) and the separate contributions from the LAE system density correlations ω_{LL} (dotted green curve), the cross-correlation $\omega_{L\Gamma}$ between the LAE system density fluctuations and the UVBG fluctuations (dot-dashed magenta curve), the UVBG fluctuation correlations $\omega_{\Gamma\Gamma}$ (long-dashed blue curve), and the UVBG fluctuation correlations excluding the source shot noise contribution $\omega_{\Gamma\Gamma,\text{nsn}}$ (dotted-long-dashed cyan curve).

τ_Q (Myr)	sample	b_L	g	χ^2
–	O18	$3.5^{+0.3}_{-0.4}$ $\left(\begin{smallmatrix} +0.6 \\ -0.8 \end{smallmatrix}\right)$	0	1.40
–	O10	5.1 ± 0.3 $\left(\begin{smallmatrix} +0.6 \\ -0.7 \end{smallmatrix}\right)$	0	10.6
10	O18	$3.4^{+0.4}_{-0.6}$ $\left(\begin{smallmatrix} +0.8 \\ -2.0 \end{smallmatrix}\right)$	$0.40^{+0.13}_{-0.35}$ (< 0.69)	1.40
10	O10	$5.1^{+0.3}_{-0.4}$ $\left(\begin{smallmatrix} +0.6 \\ -0.8 \end{smallmatrix}\right)$	< 0.29 (< 0.49)	10.1
∞	O18	$3.4^{+0.5}_{-1.0}$ $\left(\begin{smallmatrix} +0.7 \\ -2.7 \end{smallmatrix}\right)$	$0.59^{+0.09}_{-0.39}$ (< 0.70)	1.40
∞	O10	$5.0^{+0.4}_{-0.3}$ $\left(\begin{smallmatrix} +0.7 \\ -0.8 \end{smallmatrix}\right)$	0.18 ± 0.17 (< 0.54)	10.6

Table 1. Marginalised estimates for LAE bias b_L and attenuation factor g , without UVBG fluctuations (top section; $g = 0$), for a QSO lifetime $\tau_Q = 10$ Myr (middle section) and the steady state model (∞) (bottom section). Estimates based on $w(\theta)$ are computed using the data of Ouchi et al. (2010) (O10) and Ouchi et al. (2018) (O18). Ranges are given for 68% (95%) confidence intervals or upper limits. The last column gives χ^2 for the best-fitting model.

O10 with lowest angular separation is excluded since the dark matter density fluctuations become non-linear on this scale (Ouchi et al. 2018). The best-fit models to the O10 result are found to nearly coincide with the best-fitting model with no UVBG fluctuations ($g = 0$). The best-fitting model to the O18 result has $g = 0$ for both the steady state and $\tau_Q = 10$ Myr cases. Also shown is the best-fitting model fixing $g = 0.59$, corresponding to the most likely value for g after marginalising over b_L in the steady-state model, as given in Table 1. For $g = 0.59$, χ^2 is minimum at $b_L = 2.3$. The difference from the overall best model curves shows that much of the weight of the fits comes from the data at small angle separations. This is illustrated in Fig. 3 for the model with $b_L = 2.3$ and $g = 0.59$. The curve for $\omega_{\Gamma\Gamma}$ shows that the correlations become increasingly dominated by the UVBG fluctuations on scales below 400 arcsecs. A comparison between

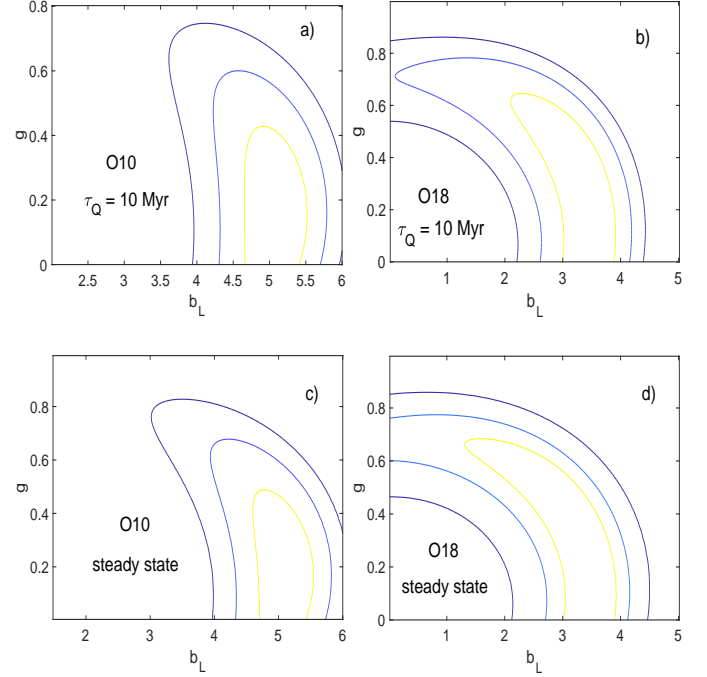


Figure 4. Likelihood contour levels in b_L and g for fits to the measured angular correlation functions at $z = 5.7$. Results shown for UVBG fluctuation models with $\tau_Q = 10$ Myr to the data from a) O10 and b) O18, and for the steady-state limit for the data from c) O10 and d) O18. (The contour levels correspond to 1σ , 2σ and 3σ enclosed probabilities.)

ω_{nsn} and the full correlation function ω shows the fluctuations are dominated by the contribution to the UVBG fluctuations from the source shot noise on scales below 100 arcsecs, given by the difference between $\omega_{\Gamma\Gamma}$ and $\omega_{\Gamma\Gamma,\text{nsn}}$. The density-dependent radiative transfer selection effect is subdominant on these scales for this model.

Likelihood contours for the fits are presented in Fig. 4. Allowing for the UVBG fluctuations opens up solutions with low LAE bias b_L and high g , particularly for the O18 data. For both the O10 and O18 data, low b_L and high g solutions become relatively more preferable for the steady state model compared with the $\tau_Q = 10$ Myr model.

The estimates for the LAE bias b_L (marginalised over g) and for g (marginalised over b_L) are displayed in Table 1 for a QSO lifetime $\tau_Q = 10$ Myr and in the steady-state limit. A bias of $b_L \approx 3.4$ is found for the O18 data, and $b_L \approx 5$ from the smaller O10 sample, with agreement at the 68% confidence level regardless of the assumed QSO lifetime, or excluding UVBG fluctuations ($g = 0$). At the 95% confidence limits, however, the solutions open up to allowing substantially reduced values for b_L with g as high as ~ 0.5 for the O10 sample and ~ 0.7 for the O18 sample.

Because much of the weight for the increased range in g arises from the correlations at small angles, and the best-fitting models lie systematically above the data points at small angles (see Fig. 2), we also provide results using an alternative fitting approach based on allowing for possible underestimates in the error bars following Hogg et al. (2010). For the steady-state model fit to the O10 sample, the model parameter expectation values and 68% (95%)

confidence intervals obtained are $b_L = 5.0_{-0.6}^{+0.4}$ ($_{-1.2}^{+0.5}$) and $g = 0.32_{-0.21}^{+0.24}$ ($_{-0.27}^{+0.32}$), while for the O18 sample, the expectation values obtained are $b_L = 3.2_{-1.3}^{+0.6}$ ($_{-2.4}^{+0.8}$) and $g = 0.46 \pm 0.28$ ($_{-0.41}^{+0.32}$). These are comparable to the values found from the more direct maximum likelihood approach above, although with somewhat extended error bars allowing for a larger contribution from UVBG fluctuations. See the Appendix for further details.

4 DISCUSSION

Whilst UVBG fluctuations are too small to affect the clustering of LAEs at redshifts $z < 5$, allowing for UVBG fluctuations at higher redshifts is found to open up the LAE bias factors inferred from LAE clustering to a broader range, especially at the 95% confidence interval (CI) level. Assuming no UVBG fluctuations ($g = 0$) at $z = 5.7$, we find $b_L \simeq 3.5 \pm 0.3$ ($_{-0.8}^{+0.6}$, 95% CI) using the O18 LAE sample, and $b_L \simeq 5.1 \pm 0.3$ ($_{-0.7}^{+0.6}$, 95% CI) using the O10 sample. Allowing for UVBG fluctuations broadens the error ranges to $b_L \simeq 3.4_{-0.8}^{+0.5}$ ($_{-2.3}^{+0.7}$, 95% CI) for the O18 sample, and $b_L \simeq 5.0 \pm 0.3$ (± 0.7 , 95% CI) for the O10 sample. At the 95% confidence level, the angular correlations at angular separations smaller than 400 arcsecs may be dominated by UVBG fluctuations, allowing for solutions with much reduced LAE bias factors, especially for the larger O18 sample.

The evolution in the bias factors has been used to infer the nature of the haloes in which LAE systems reside. For a fixed halo mass, the bias factor increases rapidly with redshift. On this interpretation, the evolution in bias factors suggests LAEs occupy haloes in the mass range $10^{10} - 10^{12} M_\odot$ at $z > 2$ and may be the progenitors of present-day massive elliptical galaxies (Ouchi et al. 2020). There is, however, considerable scatter of unclear origin in the redshift trend of the bias factors. Whilst contamination by randomly distributed sources would reduce the inferred bias factors, it has also been suggested that the small volumes of some of the surveys may result in a large scatter from cosmic variance, particularly if a protocluster is in the field (Ouchi et al. 2010; Kusakabe et al. 2018). A protocluster containing luminous photoionizing sources may also increase the Ly α transmission of nearby LAEs, enhancing their clustering. For the O18 samples at $z = 5.7$, the findings here suggest low bias factors $b_L \sim 2$ may be consistent with the angular correlation strengths in the presence of a large UVBG fluctuation contribution. In this case, the evolution of the bias factor of LAEs is consistent with a constant halo mass of about $10^{10.5} M_\odot$ (see fig.16 of Ouchi et al. 2020).

The statistical limits on g are very broad. The 68% confidence levels nearly include $g = 0$. For the O18 sample, the overall best-fitting models are for $g = 0$. Nonetheless, values as high as $g < 0.7$ are acceptable at the 95% confidence level for the O18 sample, and $g < 0.5$ for the O10 sample.

The upper limits on g of 0.5–0.7 correspond to upper limits on the blueward velocity offset of $3-3.4\sigma_l$, where σ_l is the line width of the emission line, for the LAE emission compared with the Ly α attenuation edge of the surrounding gas. This corresponds to the higher values found in the simulations of Laursen et al. (2011) for $\sigma_l \approx 100 - 150 \text{ km s}^{-1}$ in an early reionization model ($z_{\text{ri}} = 10$), but are typical for late cosmic reionization ($z_{\text{ri}} = 6$). Values of $g \simeq 0.05 - 0.1$ correspond

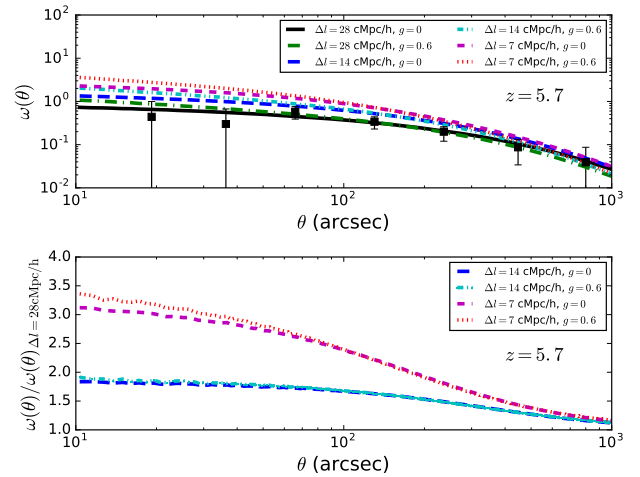


Figure 5. Dependence of the angular correlation function on width of the redshift shell. Upper panel: Angular correlation function without ($b = 3.5$, $g = 0$) and with ($b = 2.3$, $g = 0.6$) UVBG fluctuations in the steady-state limit, for shell widths of 28, 14 and 7 h^{-1} Mpc (comoving). The data points are from Ouchi et al. (2018). Lower panel: The ratio of the angular correlation functions for shell widths of 14 and 7 h^{-1} Mpc, to the correlation functions for 28 h^{-1} Mpc.

to blueward displacements of the LAE emission line of $0.9 - 1.5\sigma_l$, typical for early reionization.

The angular correlation function on small scales is suppressed by the finite width of the redshift shell imposed by the narrow-band filter centred on the Ly α wavelength for a given redshift. The width of the redshift shell at $z = 5.7$ corresponds to an averaging of the spatial correlation function up to separations of nearly $30h^{-1}$ Mpc (comoving). As a possible means of distinguishing between a correlation function dominated by the (biased) underlying dark matter density fluctuation field and by the UVBG fluctuations, we show in Fig. 5 the effect of choosing narrower filters corresponding to a half and a quarter of the actual filter width. Using the best-fit models without and with UVBG fluctuations for the steady state model, the resulting trends are virtually identical for the O10 data and exactly identical for the O18 data (since the best-fit model allowing UVBG fluctuations has $g = 0$). For this reason, we show instead the trend for the best-fit model for the most likely value of g , corresponding to $b_L = 2.3$ and $g = 0.59$, for the O18 data. For this model, UVBG fluctuations dominate the angular correlations on angular scales smaller than 400 arcsecs, with the shot noise contribution dominating on scales smaller than 100 arcsecs. Whilst reducing the thickness of the redshift shell increases the strength of the correlations (upper panel), the trends are nearly identical whether or not UVBG fluctuations dominate the correlations (lower panel). A small difference may be distinguished for the quarter-width filter case, but this would require measuring the correlations on these scales to better than 10% accuracy.

On the other hand, the result shows that the rise in the strength of the angular correlations is robust when subsamples analysed are confined to increasingly narrow redshift ranges. This provides a test of the possible contribution of contaminating sources to the angular correlations. Although spectroscopic follow-up suggests a contamination rate of only

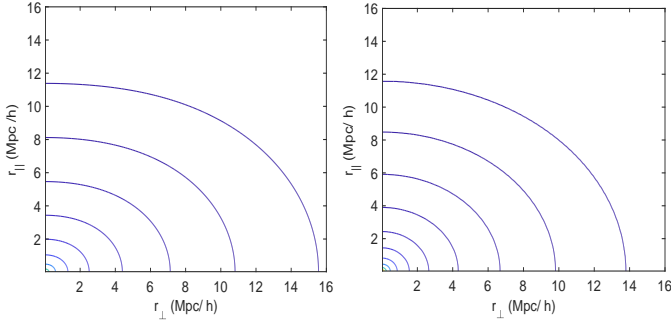


Figure 6. Contour levels of the spatial correlation function $\xi(r_{\parallel}, r_{\perp})$, as a function of the separations r_{\parallel} along the line of sight and r_{\perp} transverse to the line of sight (in comoving Mpc/h). Left panel: The best fit model to the O18 data for no UVBG fluctuations ($b_L = 3.5$). Right panel: The steady-state UVBG fluctuation model with $b_L = 2.3$ and $g = 0.59$. (The outermost contour level is 0.1, and the levels increase inward by multiplicative steps of 1.89.)

$\sim 8\%$ by foreground objects (Ouchi et al. 2018), if they cluster more strongly than the LAE systems, they would alter the expected scaling of the angular correlation function with filter width.³

The availability of a large spectroscopic sample would offer the possibility of measuring the spatial correlation function $\xi(r_{\parallel}, r_{\perp})$ as a function of line-of-sight r_{\parallel} and transverse r_{\perp} separations. Fig. 6 shows $\xi(r_{\parallel}, r_{\perp})$ for the best-fit model without UVBG fluctuations to the O18 data, with $b_L = 3.5$ (left panel) and the steady-state UVBG model with $b_L = 2.3$ and $g = 0.59$ (right panel). The angular correlation functions (Fig. 2), are nearly identical. The UVBG fluctuations tend to isotropise $\xi(r_{\parallel}, r_{\perp})$ compared with the expectation for a biased halo model. Distinguishing the two models, however, would require high precision redshift determinations.

5 CONCLUSIONS

We summarise our principal conclusions:

1. Allowing for UVBG fluctuations opens up a broader range of acceptable models for the bias factor of LAEs. For the expected range in redshifted foreground IGM Ly α photon attenuation as may arise from cosmic infall around the LAE systems in a reionized IGM, UVBG fluctuations may non-negligibly contribute to the clustering of LAEs at $z > 5$ as measured by the angular correlation function.

2. Comparison with the measured angular correlation function of LAEs in the SILVERRUSH Subaru survey at $z \simeq 5.7$ shows that, whilst the clustering is statistically consistent with no contribution from UVBG fluctuations, the measured clustering also supports models with a substantial contribution from UVBG fluctuations. These include models in which the UVBG fluctuations dominate the clustering signal over angular separations smaller than a few hundred arcseconds, corresponding to projected separations smaller than $15h^{-1}$ Mpc (comoving). On scales smaller than 100 arcsecs

³ If the foreground objects are weakly or un-clustered, however, they only dilute the measured correlations and the scaling would remain unaffected.

(about $3h^{-1}$ Mpc), the shot noise contribution to the UVBG fluctuations dominates the correlations in these models. The scales over which shot noise dominates is smaller for QSO lifetimes shorter than 10 Myr.

3. It may be possible to distinguish models with and without a substantial contribution from UVBG fluctuations to the clustering of LAEs if the angular correlation function may be measured to 10% accuracy on angular scales 10–100 arcsec at $z \simeq 5.7$. Another approach may be to measure the spatial correlations as a function of line-of-sight and transverse separations, as the UVBG fluctuations tend to isotropise the correlations.

There is much room for improving the constraint on the contribution of UVBG fluctuations to the clustering of LAE systems at high redshift. The estimate provided here made several simplifying assumptions concerning the luminosity distribution of the LAEs, their emission line widths and the velocity offset of the emission region relative to the Ly α attenuation edge of the surrounding gas. Our main conclusion is that UVBG fluctuations are sufficiently large that they may comprise a significant contribution to the overall LAE clustering strength at $z > 5$ even after the IGM has been reionized. UVBG fluctuations may continue to contribute to the clustering of LAEs into the reionization epoch as well, requiring an extension to models of the role of reionization on the LAE correlation function. More precise measurements of the LAE correlation function would better constrain the UVBG fluctuation contribution both during and after reionization completes, which in turn may help clarify the properties of the gaseous environment of LAE systems, their feedback on it, and of the nature of the LAE systems themselves.

ACKNOWLEDGEMENTS

We thank Joanne Cohn and Martin White for helpful discussions, and the anonymous referee for comments that improved the presentation. TS gratefully acknowledges support from the UK Science and Technology Facilities Council, Consolidated Grant ST/R000972/1.

This research made use of the python packages `emcee` (Foreman-Mackey et al. 2013) and `corner.py` (Foreman-Mackey 2016).

DATA AVAILABILITY

All data used in this paper are publicly available from the cited references.

REFERENCES

- Becker G. D., Bolton J. S., Madau P., Pettini M., Ryan-Weber E. V., Venemans B. P., 2015, *MNRAS*, **447**, 3402
 Becker G. D., Davies F. B., Furlanetto S. R., Malkan M. A., Boera E., Douglass C., 2018, *ApJ*, **863**, 92
 Becker G. D., D’Aloisio A., Christenson H. M., Zhu Y., Worseck G., Bolton J. S., 2021, *MNRAS*, **508**, 1853
 Bielby R., et al., 2013, *MNRAS*, **430**, 425
 Bosman S. E. I., Fan X., Jiang L., Reed S., Matsuoka Y., Becker G., Haehnelt M., 2018, *MNRAS*, **479**, 1055
 Bosman S. E. I., et al., 2022, *MNRAS*, **514**, 55
 Bouwens R. J., et al., 2015, *ApJ*, **803**, 34

- Byrohl C., Saito S., Behrens C., 2019, *MNRAS*, **489**, 3472
- Dijkstra M., Haiman Z., Spaans M., 2006, *ApJ*, **649**, 14
- Dijkstra M., Mesinger A., Wyithe J. S. B., 2011, *MNRAS*, **414**, 2139
- Foreman-Mackey D., 2016, *Journal of Open Source Software*, **1**, 24
- Foreman-Mackey D., Hogg D. W., Lang D., Goodman J., 2013, *PASP*, **125**, 306
- Furlanetto S. R., Zaldarriaga M., Hernquist L., 2006, *MNRAS*, **365**, 1012
- Gontcho A Gontcho S., Miralda-Escudé J., Busca N. G., 2014, *MNRAS*, **442**, 187
- Goto H., et al., 2021, *ApJ*, **923**, 229
- Gurung-López S., Orsi Á. A., Bonoli S., Padilla N., Lacey C. G., Baugh C. M., 2020, *MNRAS*, **491**, 3266
- Hamilton A. J. S., 1998, in Hamilton D., ed., *Astrophysics and Space Science Library Vol. 231, The Evolving Universe*. p. 185, doi:10.1007/978-94-011-4960-0_17
- Harrington J. P., 1973, *MNRAS*, **162**, 43
- Hayes M. J., Runholm A., Gronke M., Scarlata C., 2021, *ApJ*, **908**, 36
- Hogg D. W., Bovy J., Lang D., 2010, arXiv e-prints, p. arXiv:1008.4686
- Hu E. M., McMahon R. G., 1996, *Nature*, **382**, 231
- Iliev I. T., Shapiro P. R., McDonald P., Mellema G., Pen U.-L., 2008, *MNRAS*, **391**, 63
- Itoh R., et al., 2018, *ApJ*, **867**, 46
- Kaiser N., 1987, *MNRAS*, **227**, 1
- Keating L. C., Weinberger L. H., Kulkarni G., Haehnelt M. G., Chardin J., Aubert D., 2020, *MNRAS*, **491**, 1736
- Konno A., et al., 2018, *PASJ*, **70**, S16
- Kulkarni G., Keating L. C., Haehnelt M. G., Bosman S. E. I., Puchwein E., Chardin J., Aubert D., 2019a, *MNRAS*, **485**, L24
- Kulkarni G., Worseck G., Hennawi J. F., 2019b, *MNRAS*, **488**, 1035
- Kusakabe H., et al., 2018, *PASJ*, **70**, 4
- Laurent P., et al., 2017, *Journal of Cosmology and Astro-Particle Physics*, **2017**, 017
- Laursen P., Sommer-Larsen J., Razoumov A. O., 2011, *ApJ*, **728**, 52
- Mason C. A., Treu T., Dijkstra M., Mesinger A., Trenti M., Pentericci L., de Barros S., Vanzella E., 2018, *ApJ*, **856**, 2
- McLinden E. M., et al., 2011, *ApJ*, **730**, 136
- McQuinn M., Hernquist L., Zaldarriaga M., Dutta S., 2007, *MNRAS*, **381**, 75
- Meiksin A. A., 2009, *Reviews of Modern Physics*, **81**, 1405
- Meiksin A., 2020, *MNRAS*, **491**, 4884
- Meiksin A., McQuinn M., 2019, *MNRAS*, **482**, 4777
- Nasir F., D’Aloisio A., 2020, *MNRAS*, **494**, 3080
- Ouchi M., et al., 2003, *ApJ*, **582**, 60
- Ouchi M., et al., 2005, *ApJ*, **635**, L117
- Ouchi M., et al., 2008, *ApJS*, **176**, 301
- Ouchi M., et al., 2010, *ApJ*, **723**, 869
- Ouchi M., et al., 2018, *PASJ*, **70**, S13
- Ouchi M., Ono Y., Shibuya T., 2020, *ARA&A*, **58**, 617
- Pascarella S. M., Windhorst R. A., Keel W. C., Odewahn S. C., 1996, *Nature*, **383**, 45
- Planck Collaboration 2020, *A&A*, **641**, A6
- Pontzen A., 2014, *Phys. Rev. D*, **89**, 083010
- Suarez T., Pontzen A., 2017, *MNRAS*, **472**, 2643
- Verhamme A., Schaerer D., Maselli A., 2006, *A&A*, **460**, 397
- Verhamme A., Dubois Y., Blaizot J., Garel T., Bacon R., Devriendt J., Guiderdoni B., Slyz A., 2012, *A&A*, **546**, A111
- Verhamme A., et al., 2018, *MNRAS*, **478**, L60
- Weinberger L. H., Kulkarni G., Haehnelt M. G., Choudhury T. R., Puchwein E., 2018, *MNRAS*, **479**, 2564
- Worseck G., et al., 2014, *MNRAS*, **445**, 1745
- Wyithe J. S. B., Dijkstra M., 2011, *MNRAS*, **415**, 3929
- Yang J., et al., 2020, *ApJ*, **904**, 26

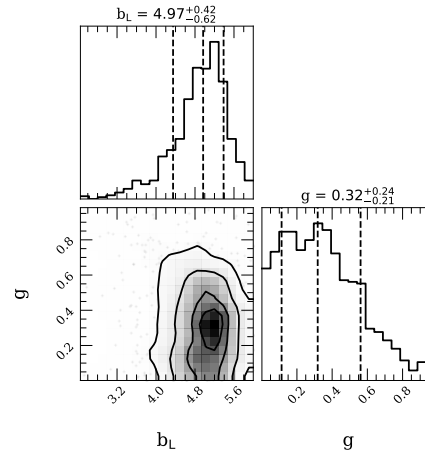


Figure A1. MCMC parameters fits for the O10 sample. Lower left panel: Likelihood function for b_L and g , marginalised over f . Upper panel: Probability density for b_L , marginalised over g and f . Lower right panel: Probability density for g , marginalised over b_L and f . The dashed lines in the probability distribution plots indicate the expectation values and 68% confidence intervals.

Zheng Z., Cen R., Trac H., Miralda-Escudé J., 2011, *ApJ*, **726**, 38

APPENDIX A: ALTERNATIVE ERROR ESTIMATOR

Following Hogg et al. (2010), we define the likelihood as

$$\ln p(\{\omega_{d,n}\}|\{\theta_n\}, b_L, g, f) = -\frac{1}{2} \sum_n \left[\frac{(\omega_{d,n} - \omega_{m,n})^2}{s_n^2} + \ln(2\pi s_n^2) \right], \quad (\text{A1})$$

where

$$s_n^2 = \sigma_n^2 + f^2 \omega_{m,n} \quad (\text{A2})$$

for model correlation $\omega_{m,n}$ at angle θ_n , measured correlations $\omega_{d,n}$ with error σ_n , and f is a factor giving the fractional variance added in the noise model. Due to the dynamical range of the data, adding a single value to the variance would overestimate the error on the data points with small correlation strengths. Instead the variance at any give point is increased by a fraction of the correlation strength at the same point as predicted by the model. We use a uniform prior on the logarithm of f instead of f itself to force f to be non-negative.

We compute the marginalised expected values for b_L and g using the Markov Chain Monte Carlo (MCMC) python module `emcee`⁴. The resulting joint contour plots for b_L and g , marginalised over f , and the marginalised distributions for b_L and g are shown in Figs. A1 and A2 for the O10 and O18 samples, respectively. The plots were produced using the python module `corner.py`⁵.

⁴ <https://emcee.readthedocs.io/en/develop/>

⁵ <https://github.com/dfm/corner.py>

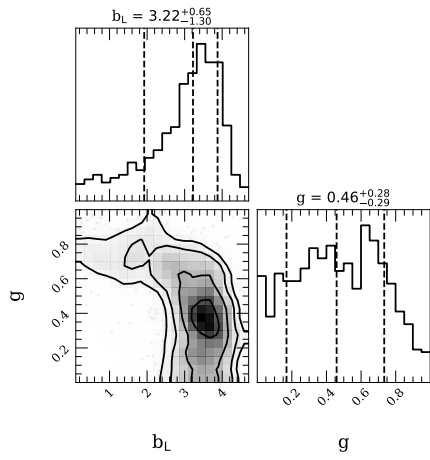


Figure A2. As for Fig. A1, but for the O18 sample.